Nature of microscopic heat carriers in nanoporous silicon

Aleandro Antidormi,[1] Xavier Cartoixà,[2] and Luciano Colombo[1,*]

[1]*Dipartimento di Fisica, Università di Cagliari, Cittadella Universitaria, I-09042 Monserrato (Ca), Italy*

[2]*Departament d'Enginyeria Electrònica, Universitat Autònoma de Barcelona, 08193 Bellaterra, Barcelona, Spain*

(Received 27 February 2018; revised manuscript received 12 April 2018; published 11 May 2018)

We performed a systematic analysis of the vibrational modes in nanoporous silicon for different values of porosity, separating them into extended modes (diffusons and propagons) and localized vibrations (locons). By calculating the density of states, the participation ratio, and the systems' dispersion curves, the spatial character of each mode as well as the effect of porosity on the thermal conductivity have been investigated. An increase of porosity is shown to promote the existence of increasingly localized modes on one side, and the progressive transformation of propagons to diffusons on the other. Finally, we provide evidence of the sizable contribution of locons to thermal transport found in large porosity samples and discuss the mechanism of energy transfer in terms of mode-mode autocorrelations and cross-correlations.

DOI: 10.1103/PhysRevMaterials.2.056001

I. INTRODUCTION

In the ongoing quest for good thermoelectric materials, which can efficiently generate electricity from heat, porous systems represent promising candidates. They generally show a large value of the figure of merit ZT, mainly due to the pore-induced reduction of lattice thermal conductivity κ with respect to their crystalline counterparts [1]. Porous silicon is among the most appealing members of this materials class, showing a thermal conductivity up to three orders of magnitude smaller than its bulk crystalline form [2]. It has consequently become the object of intense investigation not only for thermoelectric applications [1] but also in photonics [3,4] and thermal insulation [5,6]. We remark that for silicon the main contribution to thermal conductivity comes from lattice vibrations, electrons playing just a very minor role. Accordingly, hereafter we will refer—if not stated differently—to thermal conductivity actually meaning lattice thermal conductivity.

Porous samples are typically obtained by anodic etching of a monocrystalline substrate. This process is stochastic and, even under the same etching conditions and regimes, the properties of the resulting material can vary significantly. Therefore, several experimental studies have been performed on thermal conductivity, reporting a wide range of κ values, depending on doping and on fabrication techniques [7]. The lowest values $0.04 \leqslant \kappa \leqslant 1.2$ W m^{-1} K^{-1} have been achieved for p^-- and p^+-doped samples with porosity varying from 40% to 80% [8]. Tang *et al.* [9] instead focused on the thermoelectric properties of samples with cylindrical pores arranged in a hexagonal pattern, reporting that κ is reduced by a factor of 100 with respect to crystalline Si (c-Si), reaching a figure of merit of $ZT \approx 0.4$.

As for theoretical investigations, Lee *et al.* [5,10] used a combination of classical molecular dynamics (MD) and *ab initio* density functional theory to study the thermoelectric properties of nanoporous Si (np-Si) characterized by periodically arranged circular and square pores, estimating $0.6 \leqslant \kappa \leqslant 2.5$ W m^{-1} K^{-1} and $ZT = 0.4$. On the the other hand, He *et al.* [1] performed MD and lattice dynamics calculations in thin films with cylindrical pores, showing that κ could be reduced up to a factor of 20 with respect to bulk c-Si. Finally, a systematic study on lattice thermal conductivity in np-Si [11] has been addressed to work out a thorough picture of the structure-property correspondence based on atomistic simulations. In particular, the dependence of κ on the spatial distribution of pores (random or regular), their dimensions, and the overall porosity has been investigated.

Although the emerging picture is successful in reproducing the main experimental trends found for the lattice thermal conductivity, comparatively little physical insight on the microscopic nature of heat carriers has been so far provided. In particular, a robust link between the morphological features of the porous sample and its vibrational modes is still missing. Moreover, how the spatial character of such microscopic heat carriers ultimately affects the overall κ in porous silicon is still an untackled issue. In this study we provide a systematic analysis of the vibrational modes in np-Si samples as a function of porosity. Following the pioneering work by Allen and Feldman [12] on amorphous silicon, we propose for such modes a classification into extended modes (diffusons and propagons) and localized vibrations (locons). The effect of porosity on the density of states, the participation ratio, and the intrinsic character of the vibrational modes is given. Finally, the contribution of each single mode to the overall thermal conductivity is calculated, highlighting the most effective vibrations responsible for heat transport in np-Si.

The paper is organized as follows: In Sec. II the systems investigated and the computational methods employed will be described. In Sec. III we will first compute the vibrational density of states and the participation ratio. This will allow for a classification of the modes with a clear identification of locons and extendons. Finally, in Sec. IV we will calculate the overall thermal conductivity of several np-Si systems providing

*luciano.colombo@dsf.unica.it

information on the actual contribution of each mode to heat transfer. Conclusions are eventually drawn in Sec. V.

II. SAMPLE PREPARATION AND COMPUTATIONAL METHODS

In order to generate by computer np-Si samples, atoms within spherical regions with radius $R = 1$ nm have been iteratively extracted from a perfectly crystalline silicon matrix (initially containing 32 768 atoms) with cubic shape ($L = L_x = L_y = L_z \approx 87$ Å) corresponding to a $16 \times 16 \times 16$ replica of the c-Si unit cell. The dimension of the overall system has been chosen large enough to properly host all the main features of porous silicon while keeping the computational burden at a reasonable level. The position of the pores has been randomly chosen and overlap of different pores has been allowed, eventually resulting in the formation of pores with a shape other than spherical and unlike dimensions. Moreover, the number of pores was varied in order to obtain samples with different porosity, defined as

$$\varphi = \frac{V_{\text{pores}}}{V_{\text{system}}} \times 100, \tag{1}$$

where V_{system} is the total volume of the simulation box and V_{pores} is the volume occupied by the atoms removed from the crystalline matrix [13]. In this study we will consider samples with porosity varying from 5% to 40%; Fig. 1 shows the atomistic structure of the sample with 30% porosity.

After removing atoms, each configuration has been carefully relaxed using the open source LAMMPS package [14]. The actual aging of the system was differently executed depending on the kind of calculation to be performed. In particular, as explained below we needed (i) to generate zero-temperature configurations to build and diagonalize the dynamical matrix, and (ii) to run finite-temperature simulations aimed at calculating the thermal conductivity by the Green-Kubo integral. We therefore proceeded by three separated steps for each sample with given porosity. Step 1: After generating the initial pore distribution, the system was equilibrated at 300 K using a Nosé-Hoover thermostat during a 10 ns run (time step 0.5 fs); the final configuration was labeled CFG300. Step 2: In order to accomplish task (i) above, CFG300 was further quenched to zero temperature by a conjugated-gradient minimization protocol. This step was aimed at relaxing the sample to its minimum energy configuration. The resulting structure was labeled CFG0 and used to calculate the vibrational spectrum (see below). Step 3: In order to accomplish task (ii) above, CFG300 was further aged at room temperature. During this run the Green-Kubo integral was calculated (see below).

Periodic boundary conditions have been applied and the equations of motion have been integrated by the velocity-Verlet algorithm. In all our simulations, the Si-Si interaction has been described by the environment-dependent interatomic potential (EDIP) [15] which has proved to be rather accurate in describing noncrystalline forms of silicon, as required for the present investigations. In particular, EDIP reliability has been elsewhere established [11,16] in describing the thermal transport properties of disordered silicon forms, such as amorphous and nanocrystalline ones.

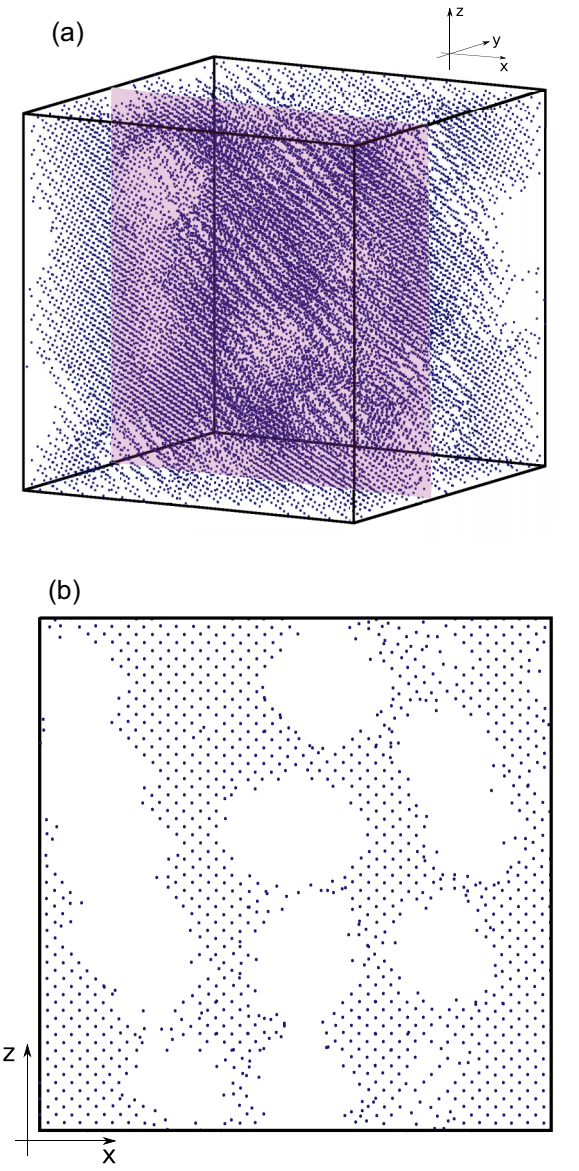

FIG. 1. Structure of the np-Si sample with 30% porosity. (a) Three-dimensional view. (b) Cross section (width 5 Å) corresponding to the highlighted plane. Atoms are shown as blue dots.

In order to study the vibrational properties of np-Si, we have constructed and diagonalized the dynamical matrix of each sample, given by

$$D_{i\alpha,j\beta} = -\frac{1}{\sqrt{m_i m_j}} \frac{\partial F_{i\alpha}}{\partial r_{j\beta}}, \tag{2}$$

where m_i is the mass of the ith atom. Hereafter we use Latin indices for labeling atoms ($i = 1,2,\ldots,N$ with N counting for the total number of atoms in the simulation cell) and Greek letters for indicating the (x,y,z) Cartesian components. Casting such a matrix in terms of the gradients of the force $F_{i\alpha}$ (i.e., the force on the ith atom along direction α caused by an infinitesimal displacement of atom j along the direction β) is a convenient formulation for a twofold reason, namely, (i) through MD we have direct access to $F_{i\alpha}$ and (ii) by Eq. (2) we need to evaluate just first-order derivatives. In

particular, the task has been numerically accomplished by finite difference with an atomic displacement as small as 5×10^{-4} Å (different displacement amplitudes resulted in a negligibly altered spectrum of $D_{i\alpha,j\beta}$). From the diagonalization of the dynamical matrix, eigenvectors $\mathbf{e}_s$ and eigenvalues ω_s^2 are obtained, where $s = 1, \ldots, 3N$ counts eigenmodes. We used the SLEPc library for matrix diagonalization [17–20]. For the systems here investigated we had $19\,000 \leqslant N \leqslant 33\,000$, corresponding to a matrix rank in the range 10^4–10^5.

III. DENSITY OF STATES AND MODES CLASSIFICATION

The vibrational density of states (VDOS) of five np-Si systems with porosity from 5% to 40% is shown in Fig. 2, where a normalized Lorentzian shape (with broadening parameter 0.01 THz) centered at each eigenfrequency has been added for a better graphical presentation. No substantial changes emerge if a different choice of the broadening parameter is made. We present results as a function of a normalized frequency $\nu^* = \nu/\nu_{\max}$, where $\nu_{\max} = 17.4$ THz is the frequency of the highest peak in c-Si VDOS (cyan in the figure) as obtained by the adopted EDIP force field. While the overestimation of $\nu_{\max}$ is a well-known feature of EDIP [21], casting all results in terms of ν^* leaves the picture emerging from the discussion reported below unaffected by such inaccuracy.

The VDOSs present peaks which are clearly reminiscent of the phonon bands of c-Si. The higher the porosity, the broader the peaks which eventually merge into a continuous VDOS without frequency gaps in the sample with $\varphi = 40\%$. This is the effect of the porosity-induced lattice disorder affecting the dynamical matrix.

For a better understanding, we proceed with a classification of the vibrational modes. Following Refs. [12,22], we compute the participation ratio (PR) defined as [23]

$$\mathrm{PR}_s \equiv \frac{1}{N} \frac{\left(\sum_{i=1}^{N} e_{i,s}^2\right)^2}{\sum_{i=1}^{N} e_{i,s}^4}. \tag{3}$$

This quantity provides a normalized estimation of the subset of atoms participating to the s-th vibrational mode. The spatial extension of such a subset is directly linked to the localized or extended character of that mode: for extended modes PR ~ 1, whereas localized modes have progressively smaller ratio, down to the limit PR $= 1/N$ for a mode completely localized on a single atom. The participation ratio for our np-Si samples is shown in Fig. 3. We remark that the unavoidable finite accuracy in the determination of the eigenvectors $\mathbf{e}_{i,s}$ makes (i) the PR calculation quite noisy and (ii) the maximum PR value definitely lower than 1 in any case. This is clearly shown by the result obtained for c-Si. All the samples considered share the same qualitative behavior, although the maximum PR is affected by the porosity: vibrations in samples with a larger φ have (at almost all frequencies) a smaller participation ratio. This implies that the ratio of atoms generally involved in each single mode is limited by the porosity of the sample. Hence, we expect that the atomic-scale architecture of the sample will play a key role in assigning the localized/extended character of the vibrational modes.

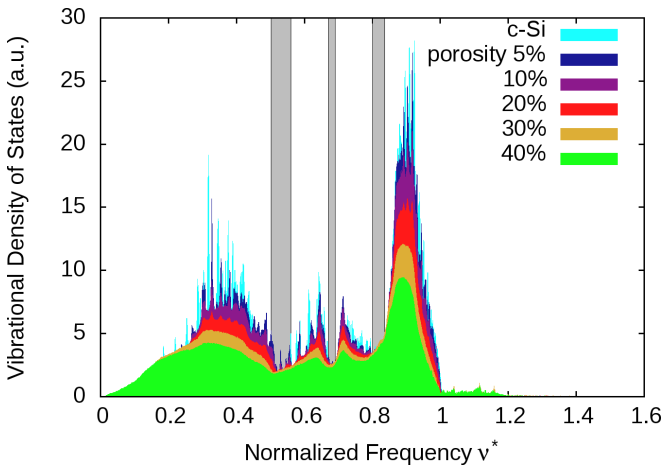

FIG. 2. The VDOS for np-Si samples with different porosity. Shaded gray areas mark the gaps separating vibrational bands. On the horizontal axis the normalized frequency $\nu^* = \nu/\nu_{\max}$.

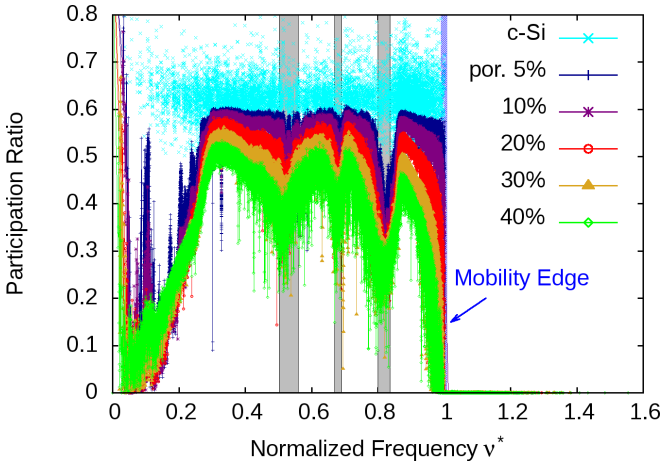

FIG. 3. Eigenmode participation ratio (PR) as a function of the normalized frequency in np-Si samples with different porosity. Shaded gray areas mark the gaps separating vibrational bands; the blue solid line marks the mobility edge.

A. Extendons vs locons and the mobility edge

Just above $\nu^* \sim 1.0$, the high-frequency behavior is characterized by a dramatic change in the participation ratio for any value of porosity considered. This marks the so-called *mobility edge*, which represents the border between extended modes (*extendons*), characterized by a high value of PR, and localized modes (*locons*) showing small values of PR [12]. The extended vs localized nature of the vibrational modes (or, equivalently, their labeling as extendons or locons, respectively) can be better appreciated when we visualize the corresponding atomic displacement field. Figure 4 shows the atomic displacements of a high-frequency locon (top panel) and a medium-frequency extendon (middle panel) in the sample with 30% porosity: red arrows superimposed to each atom denote the displacement vector (the vectors have been amplified by the same factor scale for better representation). While in the locon case, only a small fraction of atoms presents a sizable displacement, in the extendon case basically all the atoms move with respect to their equilibrium position, yet in a generally disordered

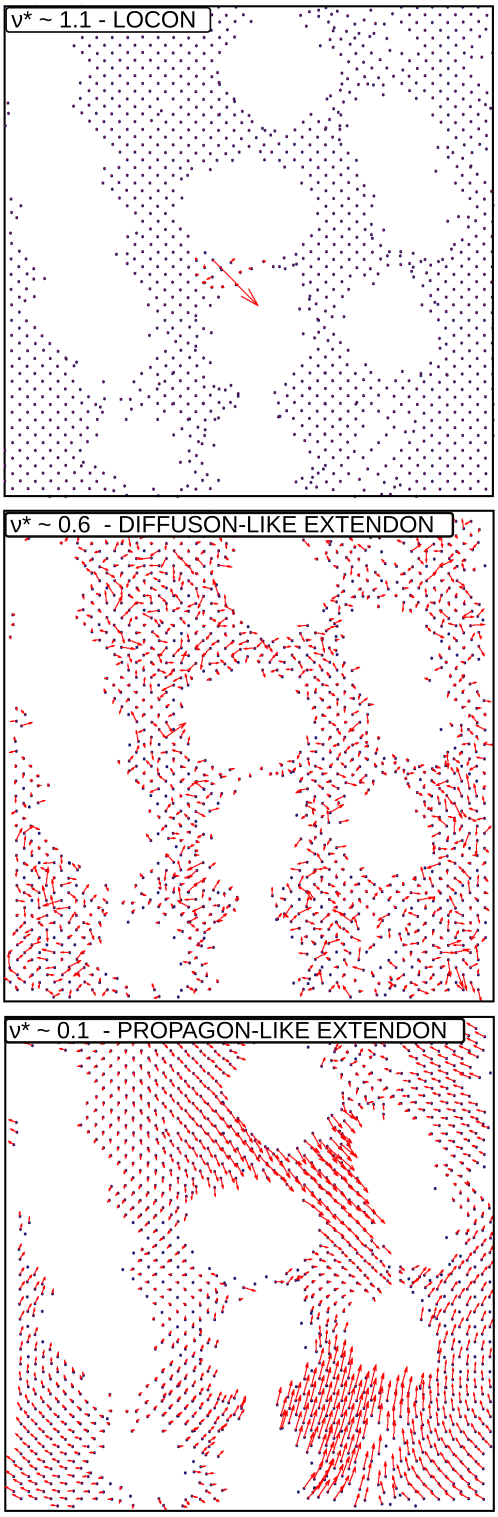

FIG. 4. Atomic displacements for three eigenmodes in the sample with 30% porosity in the section highlighted in Fig. 1. Displacements (properly scaled) are shown as red vectors superimposed on the atoms (blue dots).

fashion. For reasons explained below this mode is referred to as a *diffuson-like* extendon.

To provide additional characterization of the vibrational modes, we define according to Ref. [12] the *average coordination number*, as the weighted number of bonds with first neighbors formed in a given mode. It is calculated as

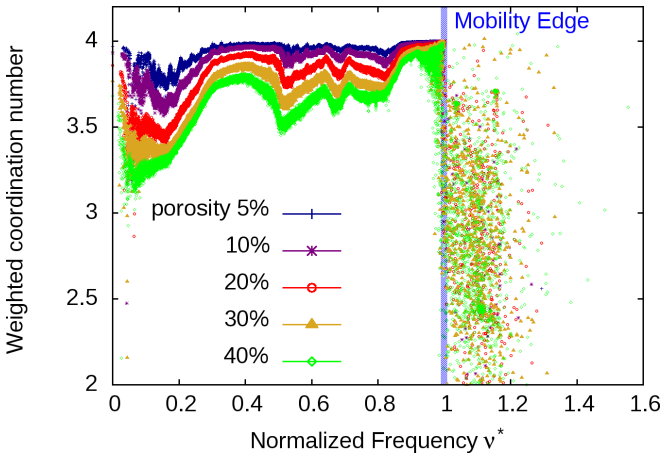

FIG. 5. The average coordination number as a function of the eigenmode normalized frequency. Minima are found at the band edges (see Fig. 2). High-frequency localized modes are characterized by very small coordination values.

$$\bar{n}_s = \frac{1}{\sum_{i=1}^{N} e_{i,s}^2} \sum_{i=1}^{N} n_{C,i} e_{i,s}^2, \tag{4}$$

where $n_{C,i}$ is the coordination number of the ith atom, and $e_{i,s}^2$ is the squared modulus of its displacement vector. To compute the $n_{C,i}$ we used a bond cutoff as small as 2.5 Å. Pores being nested into a crystalline silicon matrix, the maximum value of $\bar{n}$ is 4, with smaller values obtained for atoms located in proximity of pore surfaces.

The average coordination number as a function of frequency is shown in Fig. 5. For extended modes $\bar{n}_s$ is close to 4, while high-frequency localized modes are characterized by a comparatively much smaller value, in opposition to the overcoordinated character of locons in a-Si. This provides evidence that high-frequency locons are confined nearby the boundaries of the pores. The value of $\bar{n}$ is affected by porosity, with high φ values implying smaller coordination numbers throughout the frequency spectrum. We accordingly argue that increasing porosity determines a larger amount of undercoordinated atoms. We remark that values $\bar{n} < 3$ indicate the presence of very reactive atomic sites which are unlikely found in real systems: we guess they are an artifact of the adopted force field. Nevertheless, we remark that their number is very limited and, therefore, the local occurrence of such undercoordinated atoms is not expected to affect the main picture here presented.

B. Propagons vs diffusons

The low-frequency part of the spectrum is dominated by vibrational modes for which it is possible to define a wave vector, similarly to phonons in crystalline samples. Such modes can coherently propagate through the sample for distances larger than few interatomic spaces before being scattered by lattice disorder. Due to this property, they are referred to as *propagons*. Allen and Feldman [12] separated them from

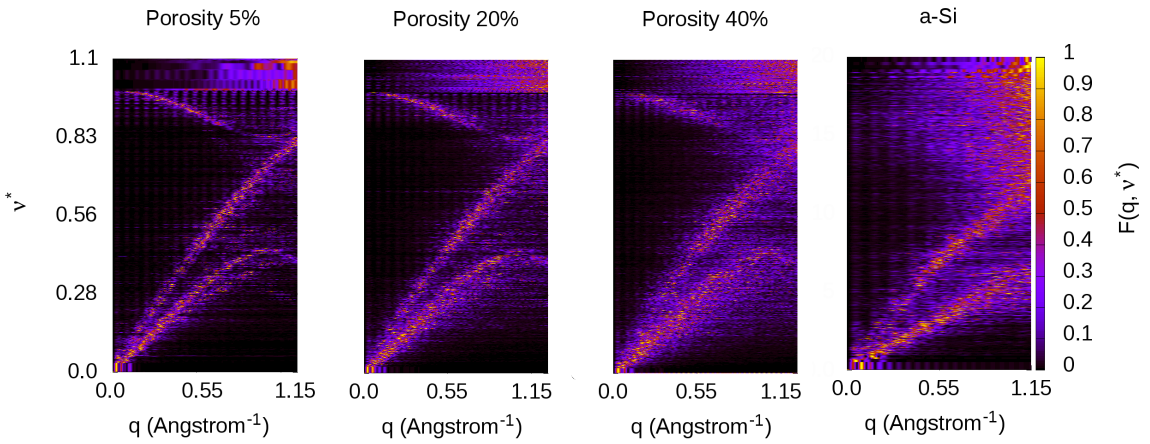

FIG. 6. Plot of the **q**-averaged $F(q,\nu^*)$ function (right scale). The contour of its maxima defines the generalized $\nu^* = \nu^*(q)$ dispersions (left scale).

diffusons, categorized as vibrational modes which are still extended but have no clear wave vector definition. While propagons generally characterize the low-frequency spectrum in amorphous materials [12], diffusons are more commonly found at high frequency. Figure 4 (bottom) shows a propagon at $\nu^* \sim 0.1$ in a sample with 30% porosity: the existence of a phase relationship between displacements of neighboring atoms is graphically evident and, accordingly, a wave vector can be defined for this mode.

In order to possibly assign a wave vector **q** to propagons, we need to follow a multistep procedure. At first we calculate the Fourier transform of the eigenvectors defined as [22]

$$F(\mathbf{q},\nu^*) = \sum_{s=1}^{3N} \left| \sum_{i=1}^{N} \mathbf{e}_{i,s}(\nu_s^*) e^{i\mathbf{q}\cdot\mathbf{R}_i} \right| \delta(\nu^* - \nu_s^*). \qquad (5)$$

In order to accomplish this task, we evaluated Eq. (5) on a $20 \times 20 \times 20$ grid of points in a cubic region with side $16 \times 2\pi/L$. Next, $F(\mathbf{q},\nu^*)$ for each single mode of frequency ν^* is averaged over all possible directions of **q**: such a **q**-averaged quantity will be hereafter referred to as $F(q,\nu^*)$ and it is shown in Fig. 6 for three np-Si samples with porosity of 5%, 20%, and 40%, respectively. We also report the result of the calculations performed on a sample of a-Si. This result, obtained for a cubic cell with 8000 atoms amorphized by quench-from-the-melt (cooling rate of 0.1 K/pS, initial temperature 2000 K), is in perfect agreement with previous findings on amorphous-like materials [22]. For a better visual effect we also normalize the function in Eq. (5) by the magnitude of its maximum for each value of ν^*.

In the three cases shown, well-resolved $\nu^* = \nu^*(q)$ dispersions are found by linking all the maxima of the $F(q,\nu^*)$ function, in particular for the sample with 5% porosity, where acoustic (both transverse and longitudinal) and optical branches are clearly visible. The effect of increasing porosity is as expected: any dispersion becomes increasingly less defined, while blurred portions appear, a signature that the definition of a wave vector becomes more and more questionable. Interestingly enough, this effect does not depend on the frequency range. Hence, low-porosity np-Si inherits the dispersion curves of the crystalline matrix from which it has been derived. An increasingly larger porosity, however, affects the background translational invariance eventually driving the system to a configuration where the propagon picture is no longer valid: vibrational modes (heat carriers) do not any longer propagate coherently but, rather, diffuse through scattering events.

The main differences between a-Si and np-Si are clear. While in the former a definite frequency-resolved separation among propagons and diffusons can be identified (hence, the so-called *Ioffe-Regel limit* can be properly defined [24]), in np-Si no such distinction exists in the frequency domain: propagons dominate the whole spectrum at low φ values, gradually transforming into diffusons at larger φ.

IV. THERMAL TRANSPORT PROPERTIES

We now calculate the thermal conductivity of np-Si and determine the contribution of each mode (or class of modes, e.g., extendons and locons). To this aim we will exploit the methodology recently developed by Lv and Henry termed Green-Kubo modal analysis (GKMA) [25], a combination of the Green-Kubo (GK) formula with information on the vibrational eigenmodes extracted from the dynamical matrix. Interestingly enough, GKMA incorporates all the degrees of anharmonicity, since MD simulations are used to obtain the time history of the modal contributions to the heat current operator. More specifically, the GKMA approach relies on the projection of the anharmonic atomic trajectories onto the eigenmodes with no previous assumptions on the nature of the modes involved. Under this respect GKMA allows us to compute the mode contributions to the overall heat current operator only from the knowledge of the atomic velocity field. It is important to note that this method describes thermal transport in terms of correlation rather than scattering. The method has been successfully applied to crystalline silicon, amorphous silicon [25], and amorphous carbon [26], yielding good agreement with other modal analysis methods and experimental data. While the details of GKMA are given in Ref. [25], here we briefly summarize its formalism to support the interpretation of our results.

The key GKMA quantity is the single-mode heat flux operator $\mathbf{Q}_s(t)$ [27], which is given by

$$\mathbf{Q}_s(t) = \frac{1}{\Omega}\sum_{i=1}^{N}\left[E_i\dot{\mathbf{x}}_i(s,t) + \sum_{k=1}^{N}[\mathbf{F}_{ik}\cdot\dot{\mathbf{x}}_i(s,t)]\mathbf{r}_{ik}\right], \quad (6)$$

where E_i is the sum of the potential and kinetic energy of atom i, Ω is the volume of the simulation cell, and $\mathbf{r}_{ik}$ is the distance between atoms i and k. Moreover, $\mathbf{F}_{ik}$ indicates the force on the ith atom upon a displacement of the kth atom. The quantity $\dot{\mathbf{x}}_i(s,t)$ represents the s-mode contribution to the velocity of the i-th atom: it is obtained on-the-fly during a constant-energy MD run by projecting the predicted atomic velocities onto the basis set provided by the eigenvectors of the dynamical matrix, i.e., $\dot{\mathbf{x}}_i(s,t) = [\mathbf{v}_i(t)\cdot\mathbf{e}_{i,s}]\mathbf{e}_{i,s}$. The thermal conductivity of the system can be calculated by replacing the above expression for the heat flux in the usual Green-Kubo formula

$$\kappa = \frac{\Omega}{3k_BT^2}\int_0^\infty\left\langle\sum_{s=1}^{3N}\mathbf{Q}_s(t)\cdot\sum_{s'=1}^{3N}\mathbf{Q}_{s'}(0)\right\rangle dt \quad (7)$$

$$= \frac{\Omega}{3k_BT^2}\sum_{s,s'=1}^{3N}\int_0^\infty\langle\mathbf{Q}_s(t)\cdot\mathbf{Q}_{s'}(0)\rangle dt, \quad (8)$$

where k_B is the Boltzmann constant and T is the temperature. These equations express the thermal conductivity as a double summation over individual mode-mode heat flux cross-correlation functions. They weight the contribution to κ of any single correlation between pairs of modes. According to this picture thermal conductivity is cast in terms of correlations rather than scattering. One can also recast the previous equation as a direct summation over single-mode thermal conductivities $\kappa(s)$

$$\kappa = \sum_{s=1}^{3N}\frac{\Omega}{3k_BT^2}\int_0^\infty\langle\mathbf{Q}_s(t)\cdot\mathbf{Q}(0)\rangle dt = \sum_{s=1}^{3N}\kappa(s), \quad (9)$$

where $\mathbf{Q}(0) = \sum_{s=1}^{3N}\mathbf{Q}_s(0)$. It is important to acknowledge that such a decomposition of κ into single-mode terms is by no means unique and other ways could be as well adopted. Nonetheless, we will hereafter consider only decomposition in Eq. (9), since it has proved to faithfully reproduce the modal contribution in c-Si [25]. We remark that, by their very definition, single-mode contributions can be either positive or negative.

In order to deal with systems at temperature lower than the Debye temperature, we modified Eq. (9) by applying quantum heat capacity corrections, i.e., replacing the classical Dulong-Petit specific heat $c_{DP}(\omega) = k_B/\Omega$ by its quantum counterpart $c_q(\omega) = \frac{k_Bx^2\exp(x)}{\Omega[\exp(x)-1]^2}$, where $x = h\omega/(k_BT)$ [28]. Hence, we multiplied each term in Eq. (9) by the quantity $c_q(\omega)/c_{DP}(\omega)$ [26].

As a sanity check of the present procedure adopted for predicting κ, we first show in Fig. 7 the result of thermal conductivity calculation for np-Si at 300 K as a function of φ. An exponential decrease of κ is observed, highlighting how porosity detrimentally affects thermal transport. The trend that we obtained is in good agreement with other calculations on analogous systems [11] using the same empirical EDIP potential. Present results are compared to an effective model

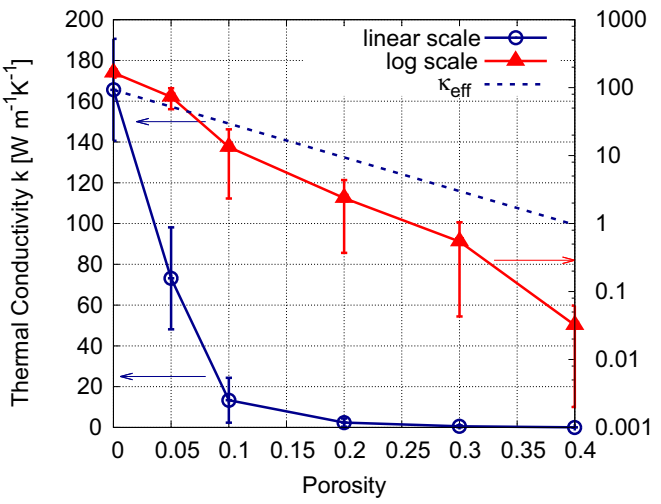

FIG. 7. Calculated thermal conductivity of the np-Si systems at $T = 300$ K as a function of porosity: linear scale in blue, logarithmic scale in red solid lines. The blue dashed line is the effective thermal conductivity κ_{eff} predicted in Ref. [11] by solely taking into account the reduction in the atom number.

taking solely into account the effect of number of modes reduction due to the removal of atoms from the simulation cell (dashed blue line in Fig. 7): we argue that such an observed large difference clearly indicates that pores affect the overall thermal conductivity to a much larger extent than that due to the decrease in the number of modes alone. Moreover, the value of κ for c-Si (160 W m^{-1} K^{-1}) shows excellent agreement with the one reported in Ref. [29], although as already known it is larger than the experimental one (140 W m^{-1} K^{-1}), a feature attributed to the EDIP potential. To calculate the Green-Kubo integral in Eq. (9), equilibrium MD simulations were performed: after equilibrating the systems previously generated (see Sec. II) for 2 ns at $T = 300$ K (with 0.5 fs time step), correlations of the heat fluxes in Eq. (9) have been sampled during a 10-ns-long simulation. The maximum value chosen for the correlation time was 1 ns. In order to improve the statistics, we averaged over three different trajectories, where different initial conditions for the atomic velocity distributions were imposed.

As a first result, we present the normalized thermal conductivity accumulation function for our np-Si systems (Fig. 8). The resulting integral values increase almost monotonically along all the frequency spectrum, allowing us to assign a specific contribution to all different kinds of modes. In this respect, we focus on the contributions of extendons (dominating the low-frequency spectrum) and locons, since we have already provided evidence that in np-Si no frequency-resolved distinction among diffusons and propagons can be made and, furthermore, large porosities imply the existence of diffusons rather than propagons. For all porosity values, extended modes determine the large part of the overall thermal conductivity. However, the most striking feature of Fig. 8 is the non-negligible contribution associated with locons, which are responsible for up to 10% of the thermal conductivity in the 40% porosity sample. This result does not support the intuitive picture that locons carry small contributions due to

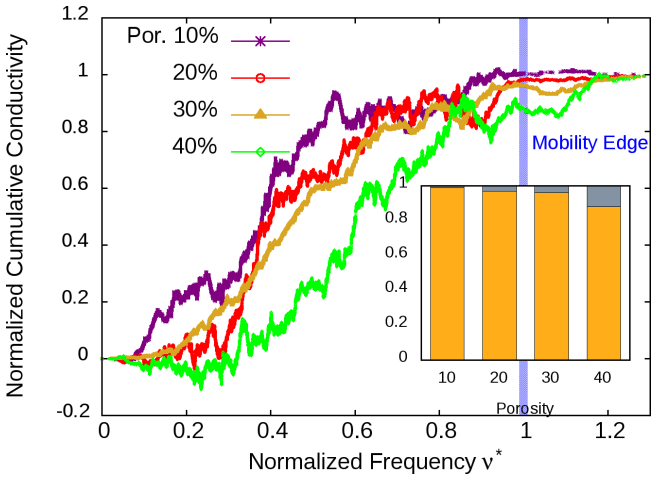

FIG. 8. Normalized cumulative κ for the systems with different porosity as function of frequency. The vertical solid line denotes the mobility edge: extended modes lie on the left, high-frequency modes on the right. In the inset, the percentage contribution of extendons (orange) and locons (gray) in the overall κ as a function of porosity is shown.

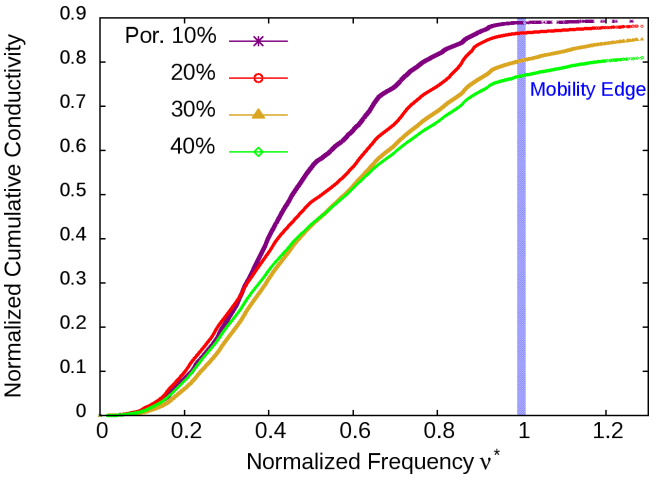

FIG. 9. Normalized thermal conductivity accumulation function due to mode-mode autocorrelations only for systems with different porosity as function of frequency. The vertical solid line denotes the mobility edge.

their restricted spatial extent. It is important to acknowledge that an unexpectedly sizable locon contribution was recently found also in a-SiO_2 [30]. Interestingly, in our np-Si systems the locon contribution increases with porosity, ranging from 1% in the 10% porosity sample to 10% in 40% porosity one (see inset of Fig. 8). We argue that this is primarily due to the fact that locons constitute an increasing portion of the vibrational spectrum of the system when increasing porosity. Specifically, locons represent the 0.1% of the total number of modes at a 10% porosity, increasing up to 4% in the 40% sample.

Further insight can be gained by investigating the transport mechanism by means of which each mode contributes to κ. To this aim, we consider the contributions to κ arising from mode-mode autocorrelations and cross-correlations, corresponding to the $s = s'$ and $s \neq s'$ cases in Eq. (7), respectively. Specifically, it has been argued that strong mode-mode cross-correlations suggest that the two modes somehow interact strongly, frequently, or for long periods of time, and possibly in collaboration with other modes [25]. On the contrary, large autocorrelations denote a strong capability of a mode to autonomously contribute to κ. In Fig. 9 we show the accumulation thermal conductivity function due to autocorrelation terms only (the value is normalized to the absolute value of κ). For each value of porosity, autocorrelations are responsible for the largest part of thermal conductivity, up to 90% in the low-porosity samples. Furthermore, the autocorrelations of extended modes (falling below the mobility edge) are clearly larger than those of locons, as it is expected. The most important result is, however, the fact that the overall autocorrelation contributions to κ decrease with porosity: from 90% when $\varphi = 10\%$ to 75% when $\varphi = 40\%$. This points to an increasing contribution to κ due to cross-correlation terms and a consequently poorer capacity of modes to autocorrelate effectively when porosity increases. In particular, since the increase of porosity determines a mode character transformation from propagon-like to diffuson-like, this leads us to argue that diffusons autocorrelate at a smaller extent with respect to propagons.

The accumulation thermal conductivity function due to mode-mode cross-correlations is shown in Fig. 10. Cross-correlations assume both positive and negative values (in particular, we remark on the strong negative terms found for the sample with $\varphi = 40\%$), eventually summing up to a positive value when accumulation throughout the full frequency spectrum is considered. The total cross-correlation contributions of extended modes are evidently smaller than the corresponding autocorrelations for each value of porosity; this implies that their spatial delocalized character generally allows them to effectively contribute to thermal conductivity on their own. From Fig. 10 it is also possible to notice how locon (modes above the mobility edge) cross-correlations increase with porosity: the larger φ the stronger the cross-correlation

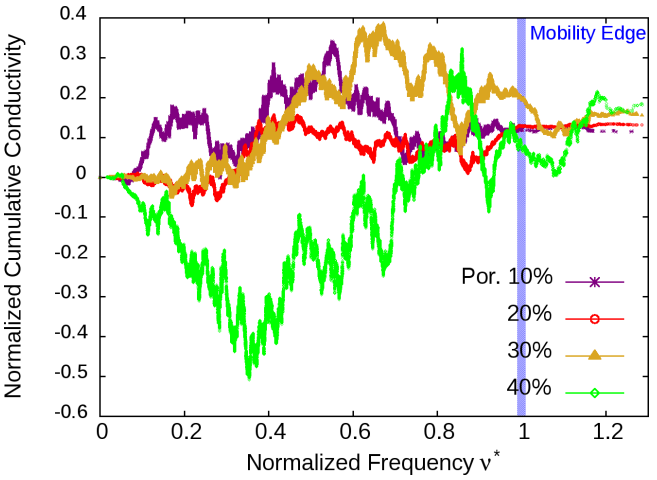

FIG. 10. Normalized thermal conductivity accumulation function due to mode-mode cross-correlations only for systems with different porosity as a function of frequency. The vertical solid line denotes the mobility edge.

contributions to κ. Moreover, their cross-correlations generally overcome the corresponding autocorrelation terms. Such a feature clarifies the fundamental mechanism by which locons contribute to thermal transport: locons serve as bridges for other modes, thus helping the process of energy transfer from one side to the other of the material.

V. CONCLUSIONS

We performed a detailed analysis of the vibrational modes of np-Si samples for different values of porosity. Starting from the knowledge of the eigenmodes and eigenfrequencies of the dynamical matrix of each system, we calculated the vibrational densities of states and characterized the modes of vibration in terms of their spatial extension. By calculating the Fourier transform of the modal atomic displacements, we also show how in porous systems propagons gradually transform into diffusons when increasing porosity. The differences with a-Si are evidenced and the impossibility to properly define a frequency separating propagons from diffusons in np-Si is discussed. Finally, we computed the contributions of each mode of vibration to the thermal conductivity, showing that porosity is responsible for a non-negligible contribution of locons (up to 10%) for systems with large porosity. Moreover, while extended modes mostly contribute to κ by correlating with themselves, locon contributions are essentially due to their interaction and correlation with other modes. This mechanism allows them to non-negligibly affect thermal transport, especially in high-porosity samples.

ACKNOWLEDGMENTS

We acknowledge financial support from the Regione Autonoma della Sardegna Basic Research Project No. CRP78744 "Energy Applications with Porous Silicon (ENAPSi)." One of us (X.C.) acknowledges Regione Autonoma della Sardegna for financial support under the initiative "Visiting Professor 2017" and the Spanish MINECO under Project No. TEC2015-67462-C2-1-R (MINECO/FEDER).

[1] Y. He, D. Donadio, J.-H. Lee, J. C. Grossman, and G. Galli, Thermal transport in nanoporous silicon: Interplay between disorder at mesoscopic and atomic scales, ACS Nano **5**, 1839 (2011).

[2] G. Gesele, J. Linsmeier, V. Drach, J. Fricke, and R. Arens-Fischer, Temperature-dependent thermal conductivity of porous silicon, J. Phys. D **30**, 2911 (1997).

[3] L. T. Canham, Silicon quantum wire array fabrication by electrochemical and chemical dissolution of wafers, Appl. Phys. Lett. **57**, 1046 (1990).

[4] J. Octavio Estevez and V. Agarwal, *Porous Silicon Photonic Crystals* (Springer International Publishing, Cham, 2014), pp. 805–814.

[5] J.-H. Lee, J. C. Grossman, J. Reed, and G. Galli, Lattice thermal conductivity of nanoporous Si: Molecular dynamics study, Appl. Phys. Lett. **91**, 223110 (2007).

[6] K. Valalaki and A. G. Nassiopoulou, Low thermal conductivity porous Si at cryogenic temperatures for cooling applications, J. Phys. D: Appl. Phys. **46**, 295101 (2013).

[7] M. J. Sailor, *Porous Silicon in Practice: Preparation, Characterization, and Applications* (John Wiley & Sons, Weinheim, 2012).

[8] W. Lang, A. Drost, P. Steiner, and H. Sandmaier, The thermal conductivity of porous silicon, MRS Proc. **358**, 561 (1994).

[9] J. Tang, H.-T. Wang, D. H. Lee, M. Fardy, Z. Huo, T. P. Russell, and P. Yang, Holey silicon as an efficient thermoelectric material, Nano Lett. **10**, 4279 (2010).

[10] J.-H. Lee, G. A. Galli, and J. C. Grossman, Nanoporous Si as an efficient thermoelectric material, Nano Lett. **8**, 3750 (2008).

[11] R. Dettori, C. Melis, X. Cartoixa, R. Rurali, and L. Colombo, Model for thermal conductivity in nanoporous silicon from atomistic simulations, Phys. Rev. B **91**, 054305 (2015).

[12] P. B. Allen, J. L. Feldman, J. Fabian, and F. Wooten, Diffusons, locons and propagons: Character of atomic vibrations in amorphous Si, Philos. Mag. B **79**, 1715 (1999).

[13] J. Rouquerol, F. Rodriguez-Reinoso, and K. S. W. Sing, *Characterization of Porous Solids II* (Elsevier, Amsterdam, 1991).

[14] S. Plimpton, Fast parallel algorithms for short-range molecular dynamics, J. Comput. Phys. **117**, 1 (1995).

[15] J. F. Justo, M. Z. Bazant, E. Kaxiras, V. V. Bulatov, and S. Yip, Interatomic potential for silicon defects and disordered phases, Phys. Rev. B **58**, 2539 (1998).

[16] C. Melis, R. Dettori, S. Vandermeulen, and L. Colombo, Calculating thermal conductivity in a transient conduction regime: Theory and implementation, Eur. Phys. J. B **87**, 96 (2014).

[17] V. Hernandez, J. E. Roman, and V. Vidal, SLEPc: A scalable and flexible toolkit for the solution of eigenvalue problems, ACM Trans. Math. Softw. **31**, 351 (2005).

[18] S. Balay, S. Abhyankar, M. F. Adams, J. Brown, P. Brune, K. Buschelman, L. Dalcin, V. Eijkhout, W. D. Gropp, D. Kaushik, M. G. Knepley, D. A. May, L. C. McInnes, K. Rupp, B. F. Smith, S. Zampini, H. Zhang, and H. Zhang, PETSc Web page, http://www.mcs.anl.gov/petsc.

[19] S. Balay, S. Abhyankar, M. F. Adams, J. Brown, P. Brune, K. Buschelman, L. Dalcin, V. Eijkhout, W. D. Gropp, D. Kaushik, M. G. Knepley, D. A. May, L. C. McInnes, K. Rupp, P. Sanan, B. F. Smith, S. Zampini, H. Zhang, and H. Zhang, PETSc users manual, Technical Report ANL-95/11, Revision 3.8, Argonne National Laboratory, 2017, URL: http://www.mcs.anl.gov/petsc.

[20] S. Balay, W. D. Gropp, L. C. McInnes, and B. F. Smith, Efficient management of parallelism in object oriented numerical software libraries, in *Modern Software Tools in Scientific Computing*, edited by E. Arge, A. M. Bruaset, and H. P. Langtangen (Birkhäuser Press, Basel, 1997), pp. 163–202.

[21] L. Sun and J. Y. Murthy, Domain size effects in molecular dynamics simulation of phonon transport in silicon, Appl. Phys. Lett. **89**, 171919 (2006).

[22] Y. M. Beltukov, C. Fusco, D. A. Parshin, and A. Tanguy, Boson peak and Ioffe-Regel criterion in amorphous siliconlike materials: The effect of bond directionality, Phys. Rev. E **93**, 023006 (2016).

[23] R. J. Bell, Vibrational properties of amorphous solids, in *Vibrational Properties of Solids*, edited by G. Gilat, Vol. 15 of

Methods in Computational Physics: Advances in Research and Applications (Elsevier, Amsterdam, 1976), pp. 215–276.

[24] Y. M. Beltukov and D. A. Parshin, Boson peak in various random-matrix models, JETP Lett. **104**, 552 (2016).

[25] W. Lv and A. Henry, Direct calculation of modal contributions to thermal conductivity via Green-Kubo modal analysis, New J. Phys. **18**, 013028 (2016).

[26] W. Lv and A. Henry, Phonon transport in amorphous carbon using Green-Kubo modal analysis, Appl. Phys. Lett. **108**, 181905 (2016).

[27] R. J. Hardy, Energy-flux operator for a lattice, Phys. Rev. **132**, 168 (1963).

[28] J. M. Ziman, *Electrons and Phonons: The Theory of Transport Phenomena in Solids* (Oxford University Press, Oxford, 1960).

[29] Y. He, I. Savic, D. Donadio, and G. Galli, Lattice thermal conductivity of semiconducting bulk materials: Atomistic simulations, Phys. Chem. Chem. Phys. **14**, 16209 (2012).

[30] W. Lv and A. Henry, Examining the validity of the phonon gas model in amorphous materials, Sci. Rep. **6**, 37675 (2016).